

Structure and crystallization kinetics of manganese lead tellurite glasses

K. A. Aly · Y. B. Saddeek · A. Dahshan

Received: 23 April 2014 / Accepted: 27 September 2014 / Published online: 21 October 2014
© Akadémiai Kiadó, Budapest, Hungary 2014

Abstract Five glass compositions were prepared by melt-quenching method with progressive substitution of ZnO for MnO₂ in the glass system 70 TeO₂-*x*ZnO-(20 - *x*) MnO₂-10 PbO (0 ≤ *x* ≤ 20 mol%). The FTIR spectra were recorded over a continuous spectral range 400–2,000 cm⁻¹ to study the structure changes with increasing of ZnO content. Differential thermal analysis was recorded to determine the glass transition temperature, *T*_g, and the crystallization temperature, *T*_p. The results indicated that the melting temperature, *T*_m, of these glasses under normal atmospheric conditions was found in the range of 1,030–1,090 K depending on the composition. The *T*_g decreased while the *T*_m increased with increasing ZnO content. The thermal parameters were correlated with the results of FTIR spectra. X-ray diffraction analysis showed that the as-prepared glasses have an amorphous nature while there are many crystalline phases such as Mn₂Te₃O₈, Mn₇O₁₅Pb₃, Pb₃Mn₇O₁₅, Pb₂Te₃O₈, Pb₂ZnTeO₆, and Zn₂PbO₄, which are formed after heat treatment.

Keywords Tellurite glasses · Infrared spectroscopy · DTA and XRD

Introduction

Study of various oxide glasses obtained by non-conventional network formers like TeO₂ and/or PbO [1–6] has received intensive attention due to their special physical properties such as high refractive index, high density [7], low transformation temperature, high thermal expansion [8], and excellent infrared transmission [9]. These glasses have wide applications in the fields of electronics, nuclear, solar energy technologies, and acoustic–optics devices [10–13]. The magnetic properties of glasses having transition metal (TM) oxides such as MnO₂ provide useful information on the different valence states and the magnetic interaction between TM ions in a vitreous matrix and the distribution mode of magnetic ions in the glass network [14]. Several studies on glasses have low concentration of manganese oxide establishing the presence of Mn²⁺ ions and MnO. The magnetic properties of such glasses [15–18] render them suitable for large practical and potential applications in many fields such as memory switching [19], electronics, and magnetic information storage [20]. Reddy et al. [21] reported that the addition of ZnO enhances the suitable applications in plasma display panels, computer monitors, and promising candidates for large area hang-on-wall TVs. ZnO can act as a glass former and enters the network with ZnO₄ structural units and as a network modifier by coordinated octahedrally the zinc ions. The structural and physical properties of glasses containing PbO at lower concentrations as a network modifier or at higher concentrations as a network former have been studied elsewhere [2].

K. A. Aly · Y. B. Saddeek
Physics Department, Faculty of Science and Arts, Khulais,
King Abdulaziz University, Jidda, Saudia Arabia

K. A. Aly (✉)
Physics Department, Faculty of Science, Al-Azhar University,
P.O. Box 71452, Assiut, Egypt
e-mail: kamalaly2001@gmail.com; Kaali5@kau.edu.sa

A. Dahshan
Department of Physics, Faculty of Science, Port Said University,
Port Said, Egypt

A. Dahshan
Physics Department, Faculty of Girls, King Khalid University,
Abha, Saudia Arabia

Thermal properties and crystallization behavior of some tellurite based glasses were studied by DTA and XRD [8, 22–24]. It was found that the addition of BaO reduces the thermal stability due to the formation of γ -TeO₂ phase [8], while addition of Nb₂O₅ enhances the thermal properties of the tellurite glasses through the formation of NbO₆ and increasing its rigidity [24].

The aim of the present work was to study the influence of ZnO on the structure and the thermal properties of the 70 TeO₂-*x*ZnO-(20 - *x*) MnO₂-10 PbO ($0 \leq x \leq 20$ mol%) glasses. The study was performed by FTIR, DTA, and XRD techniques. The system under study is of interest because both TeO₂ and PbO oxides are non-conditional glass formers and also due to their expected magnetic properties which will be undertaken in a new work.

Experimental

Five glass samples of different compositions in the glass system 70 TeO₂-*x*ZnO-(20 - *x*) MnO₂-10 PbO ($0 \leq x \leq 20$ mol%) were prepared by the melt-quenching method. The starting materials of PbO, TeO₂, MnO₂, and ZnO of AR grade were obtained from Aldrich, Glaxo, and CDH Chemical Company. Appropriate amounts of chemicals were thoroughly mixed in an agate mortar and melted in platinum crucible at 1,223 K for 1 h and then poured into a pre-heated aluminum mold.

FTIR spectroscopy was carried out at room temperature in the region from 2,000 to 400 cm⁻¹ with a resolution of 4 cm⁻¹ by a JASCO, FT/IR-430 (Japan) infrared spectrophotometer. Each powder sample weighing 1 mg was mixed with 50 mg of KBr powder in an agate mortar and then pressed into pellets form. At least two spectra for each sample were recorded in the wavenumber range of 2,000–400 cm⁻¹ with a resolution of 4 cm⁻¹, corrected for dark current noise, and normalized. The resulted spectra were curve fitted to get quantitative values for the band areas of heavily overlapped bands with a computer program Origin 8. Estimated error limit in the fitting process is about ± 2 cm⁻¹.

The crystallization behavior of glasses under non-isothermal conditions were followed by the DTA technique which was performed in a SHIMADZU DTA-50 ANALYZER (with an accuracy of ± 0.1 K) using 20 mg powdered samples with different heating rates ($\phi = 4, 8, 16, 32, \text{ and } 48$ K min⁻¹) in the temperature range of 300–1,093 K. All DTA experiments were performed in N₂ gas with Al₂O₃ powder as a reference material. The DTA analyzer was calibrated, for each heating rate, using the well-known melting temperatures and melting enthalpies of zinc and indium supplied with the instrument.

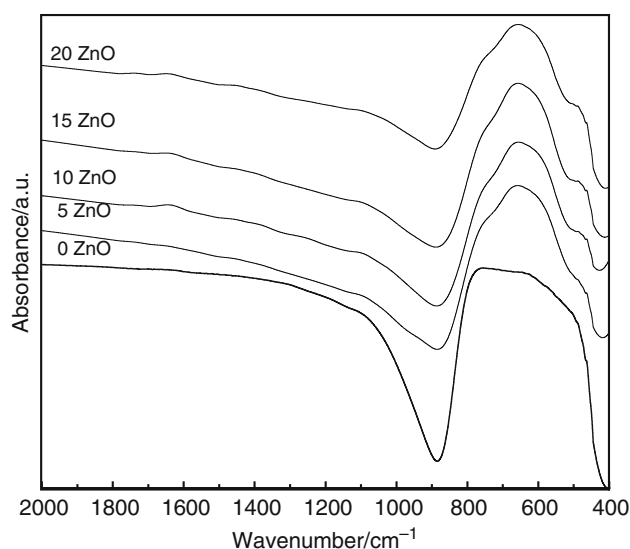


Fig. 1 Infrared spectra of the investigated 70 TeO₂-*x* ZnO-(20 - *x*) MnO₂-10 PbO ($0 \leq x \leq 20$ mol%) glasses. Numbers at the plots represent CKD content in mol%

The structure of the as-prepared and annealed glasses was checked by XRD patterns using a Philips X-ray diffractometer PW/1710 with Ni-filtered Cu K α radiation ($\lambda = 1.542$ Å), powered at 40 kV and 30 mA. The crystalline phases in each glass sample were obtained by a heat treatment at the onset temperature of the first peak of crystallization for 2 h and were identified by comparing its XRD pattern to ICDDVIEW 2006 identification cards.

Results

FTIR analysis

The recorded FTIR spectra of the studied glasses in the range of 2,000–400 cm⁻¹ shown in Fig. 1 reveal the characteristic absorption bands of tellurite glasses and a small absorption band at $\sim 1,640$ and $\sim 1,400$ cm⁻¹ attributed to the bending vibrations of O–H bonds brought by air moisture during the preparation of KBr pellets for FTIR measurements [25]. Therefore, the effective spectral domain for the structural changes concerns the range of 850–400 cm⁻¹. The main characteristics of FTIR spectra of the base glass exhibited a main absorption band with two shoulders at ~ 475 and ~ 800 cm⁻¹ which are attributed to the different structural units of TeO₂, PbO, and MnO₂. The intensity of the shoulder ~ 475 cm⁻¹ increases as the ZnO content increases. This spectrum is strongly affected by increasing the substitution of MnO₂ by ZnO. The general features of the spectra of these glasses are the shift of the position of the absorption bands to lower wavenumbers, the

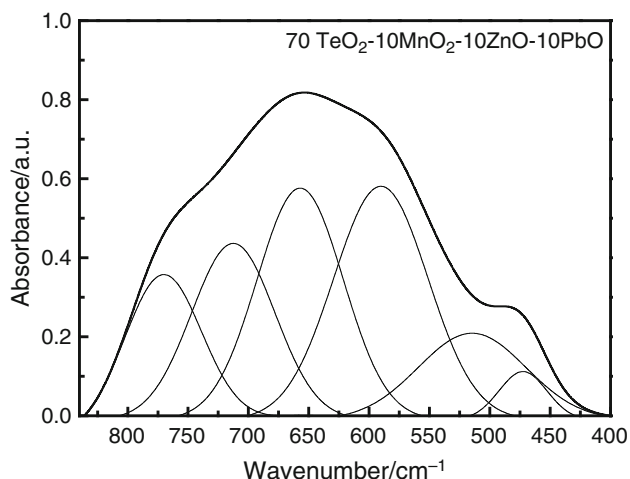


Fig. 2 Curve fitting of IR spectra of the glasses 70 TeO₂-10 ZnO-10 MnO₂-10 PbO

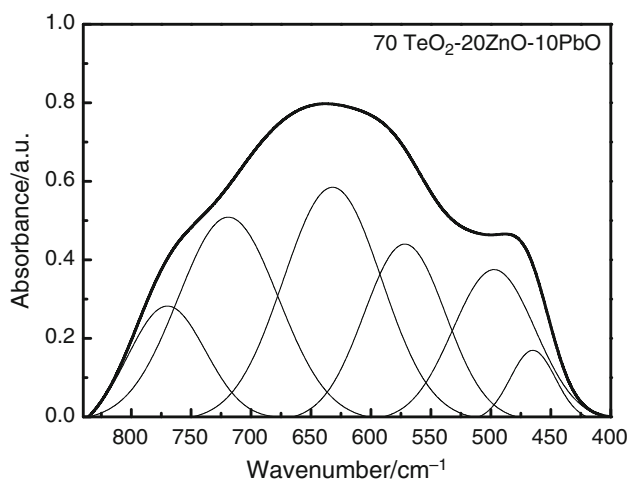


Fig. 3 Curve fitting of IR spectra of the glasses 70 TeO₂-20 ZnO-10 PbO

bands become sharp and are strongly overlapped especially in the region 500–800 cm⁻¹ as the ZnO content increases. The overlapping and broadening of the bands may be attributed to the structural grouping rearrangements with a change in glass composition, which affect the properties of glass. Therefore, a deconvolution process [26] has been applied to resolve the overlapping of the bands to identify their positions and their relative area. Figures 2 and 3 show the deconvolution of the FTIR spectra of the glasses 70 TeO₂-10ZnO-10MnO₂-10 PbO and 70 TeO₂-20 ZnO-10 PbO, respectively, as an example. Table 1 shows the characteristic parameters of FTIR absorption bands.

Thus, the peaks centered at around 473–465 cm⁻¹ can be assigned to vibrations of MnO₆ overlapped with the vibrations of ZnO₆ [27, 28]. The bands at around 515–494 cm⁻¹ were assigned to the vibration of Pb–O–Te

Table 1 Deconvolution parameters of the infrared spectra of 70 TeO₂-*x* ZnO-(20 - *x*) MnO₂-10 PbO (0 ≤ *x* ≤ 20 mol%)

0 ZnO	C	472	494	563	636	727	791
	A	4.32	17.76	18.41	20.59	27.27	11.65
5 ZnO	C	473	496	574	644	715	778
	A	3	16.86	20.35	22.83	23.33	13.63
10 ZnO	C	473	515	590	657	713	771
	A	2.89	11.62	27.61	25.02	18.43	14.42
15 ZnO	C	467	499	578	652	717	774
	A	3.5	12.35	25.64	24.22	23.2	11.09
20 ZnO	C	465	497	572	632	719	777
	A	3.86	15.05	19.45	23.78	27.64	10.22

C is the component band center (cm⁻¹) and A is the relative area (%) of the component band

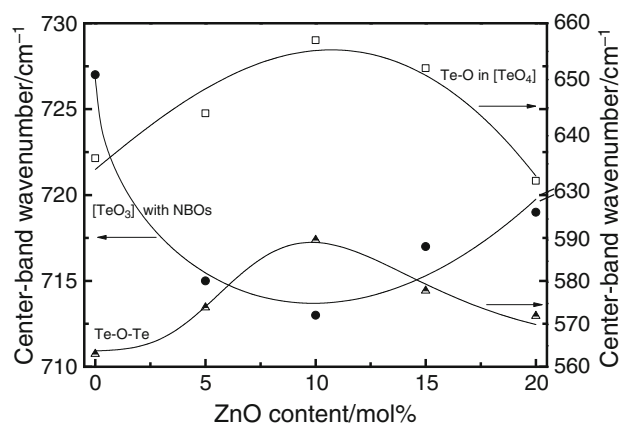


Fig. 4 Compositional dependence of the center-band wave number for vibrations of Te–O in (TeO₄), (TeO₃) and Te–O–Te in the FTIR spectra of 70 TeO₂-*x* ZnO-(20 - *x*) MnO₂-10 PbO (0 ≤ *x* ≤ 20 mol%)

[29]. The bands at 590–563 cm⁻¹ can be assigned to the bending vibrations of Te–O–Te linkages, while the bands at around 657–632 cm⁻¹ are assigned to the stretching vibration of axial Te–O bonds in the TeO₄ trigonal bipyramidal (tbp) units with bridging oxygen. The trigonal pyramid units of TeO₃ with non-bridging oxygens (NBOs) are centered located at 727–719 cm⁻¹, and the bands located at 791–771 cm⁻¹ were attributed to the stretching vibration of equatorial Te–O bonds in the TeO₄ [26, 30–32]. Figure 4 shows the compositional dependence of the center-band wavenumber on ZnO content for the effective modes of vibrations of tellurite glassy network.

X-ray diffraction (XRD) and differential thermal analyzer (DTA) analysis

The amorphous state of the as-prepared glasses was confirmed by the absence of any sharp lines or peaks in the XRD patterns as shown in Fig. 5. As a comparative

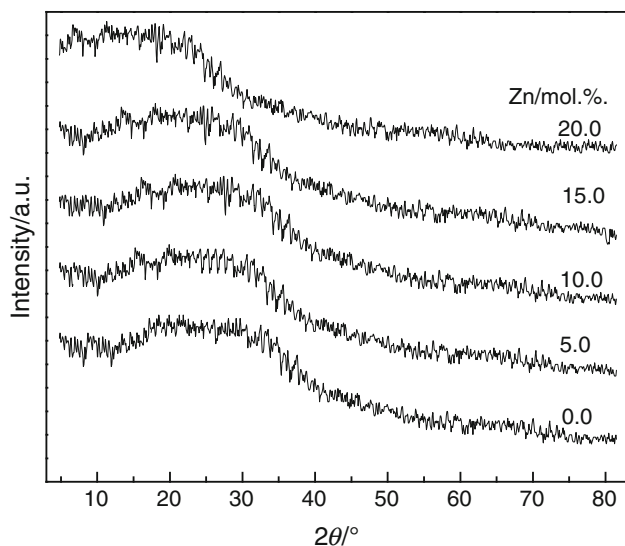


Fig. 5 XRD patterns of the 70 TeO₂-*x* ZnO-(20 - *x*) MnO₂-10 PbO (0 ≤ *x* ≤ 20 mol%) glasses

example, Fig. 6 shows the DTA curves of the 70 TeO₂-5 ZnO-15 MnO₂-10 PbO glass at different ϕ s. The glass homogeneity was revealed by the appearance of single glass transition temperature and one melting temperature. The inset of Fig. 6 represents the two overlapped crystallization peaks that were separated using Origin 8 program.

Glass transition and activation energy of glass Transition

The variation of T_g with ZnO content and heating rate for the studied glasses is shown in Fig. 7. The T_g is decreased as the ZnO content increased from 0 to 20 mol %, and increased with increasing the heating rate. The results of Fig. 7 were fitted according to the mentioned empirical relationship elsewhere [32]:

$$T_g = \delta + \Delta \ln(\phi) \quad (1)$$

where δ and Δ are constants for a given glass composition and their values are listed in Table 2.

The activation energy for glass transition E_t has been evaluated using the so-called Kissinger's formula [33]. For homogeneous crystallization with spherical nuclei [34, 35], it has been shown that the dependence of T_g on ϕ can be given by

$$\ln\left(\frac{T_g^2}{\phi}\right) = E_t/RT_g + \text{cons} \quad (2)$$

where R is the universal gas constant. Plots of $\ln(T_g^2/\phi)$ versus $10^3/T_g$ for these glasses indicated linearity for all heating rates (Fig. 8). The values of E_t decreased with the increase in ZnO content (Table 2).

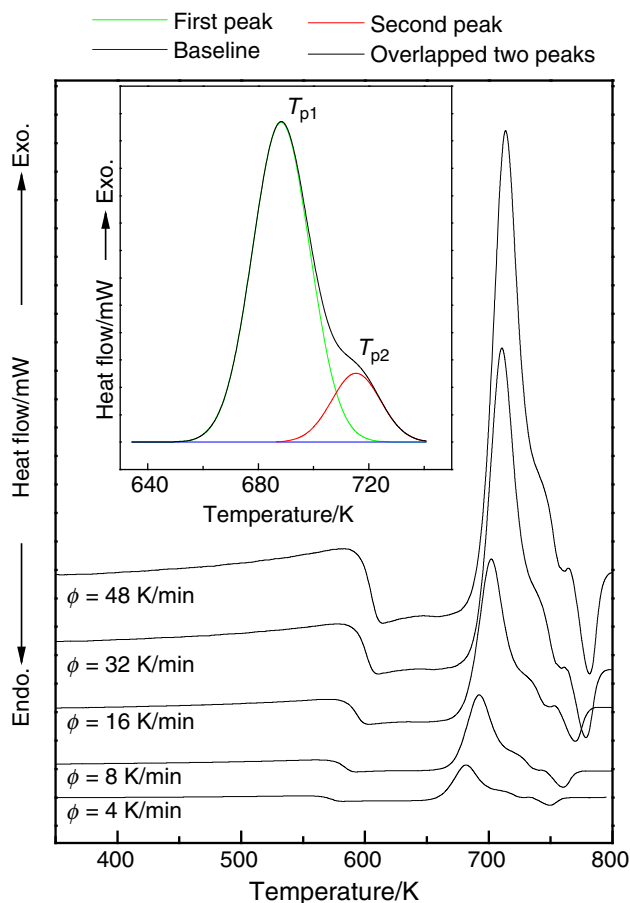


Fig. 6 a The DTA curves of the 5 ZnO-70 TeO₂-10 PbO-15 MnO₂ glass at different heating rates (ϕ) and **b** the two overlapped crystallization peak that separated using Origin 8 program

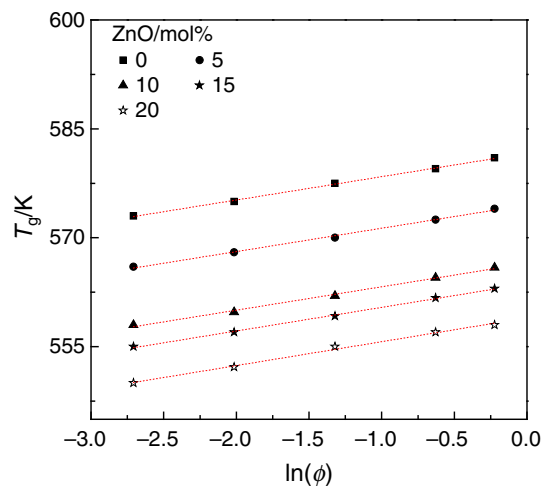


Fig. 7 The variation of T_g with ZnO content and heating rate for 70 TeO₂-*x* ZnO-(20 - *x*) MnO₂-10 PbO (0 ≤ *x* ≤ 20 mol%) glasses

Table 2 The thermal parameters $\hat{\phi}$, Δ , E_g , τ_{Tg} , E_{c1} , E_{c2} , K_{01} , K_{02} , n_1 , and n_2 for x ZnO– $(20-x)$ MnO₂– 10 PbO– $(20-x)$ MnO₂– 10 PbO– $(20-x)$ MnO₂– 10 PbO– $(20-x)$ MnO₂– 10 PbO glasses

ZnO/mol%	$\hat{\phi}$	Δ	E_g /kJ mol ⁻¹	τ_{Tg} /s	E_{c1} /kJ mol ⁻¹	E_{c2} /kJ mol ⁻¹	E_c /kJ mol ⁻¹	K_{01} /s ⁻¹	K_{02} /s ⁻¹	K_{01} /s ⁻¹	K_{02} /s ⁻¹	n_1	n_2
					Equation 3			Equation 3		Equation 4			
0	581.64	3.22	203	28.32	89.03	100.20	87.35	1.18×10^{27}	9.73×10^{28}	1.13×10^{25}	6.45×10^{27}	1.092	1.29
5	574.53	3.21	198.3	29.53	84.38	95.34	82.15	2.7×10^{24}	8.6×10^{26}	1.16×10^{22}	7.59×10^{24}	0.98	1.1
10	566.48	3.22	192	30.65	76.22	95.90	74.39	3×10^{22}	5.16×10^{27}	1.53×10^{20}	8.04×10^{25}	1.3	1.15
15	563.67	3.25	188.6	32	81.61	-	80.96	9.6×10^{23}	-	1.26×10^{22}	-	1.41	-
20	558.98	3.29	182.5	34	122.79	139.56	121.44	6.93×10^{34}	6.44×10^{38}	8.08×10^{32}	9.59×10^{35}	1.51	1.32

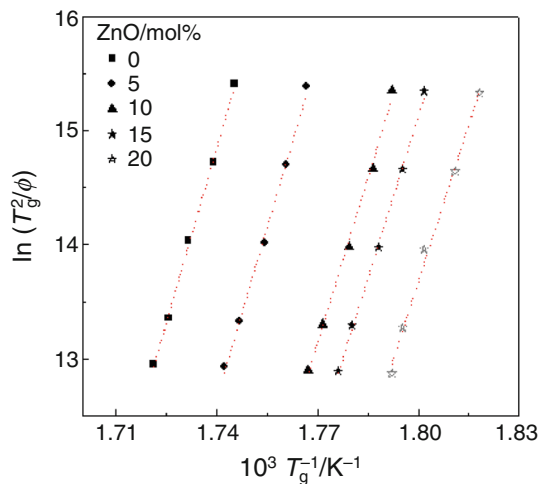


Fig. 8 The thermal parameter $\ln(T_g^2/\phi)$ versus $10^3/T_g$ for 70 TeO₂- x ZnO-($20-x$) MnO₂-10 PbO ($0 \leq x \leq 20$ mol%) glasses

Crystallization kinetics

The activation energy for crystallization (E_c) can be evaluated from the dependence of T_p on ϕ by applying Afify’s condition [36]. According to this condition when the crystallized volume fraction (χ) equals to 0.63, the value of the term $\ln(1-\chi)$ will be -1 and the Johnson–Mehl–Avrami equation can be written in the form of

$$-1^n = \ln(1 - \chi) = -(Kt)^n, \tag{3}$$

i.e.,

$$K_{0.63}t_{0.63} = 1, \tag{4}$$

where n is Avrami’s exponent, $K_{0.63}$ is the overall reaction rate that can be expressed as

$$K_{0.63} = K_0 e^{\frac{-E_c}{Rt_{0.63}}}, \tag{5}$$

where K_0 is the frequency factor, E_c is the activation energy of crystallization, and $t_{0.63}$ is the time at $\chi = 0.63$. The value of $t_{0.63}$ at each heating rate can be determined from Fig. 9 where the crystallized volume fraction was plotted as a function of temperature (a) and time (b) for the first and second peak of the glass 70 TeO₂-20 MnO₂-10 PbO as an example. The activation energy for crystallization (E_c) can be determined without the dependence on the Avrami’s exponent (n) from the slope of the linear relation between $\ln(K_{0.63})$ and $10^3/T_{0.63}$. Figure 10 investigates the values of $\ln(K_{0.63})$ as a function of $10^3/T_{0.63}$ for different glasses. The deduced values of activation energy of crystallization and frequency factor, K_0 , are listed in Table (2). Furthermore, one can use the well-known Kissinger’s formula [35] in the form of

$$\ln(T_p^2/\phi) = E_c/RT_p - \ln(K_0R/E_c). \tag{6}$$

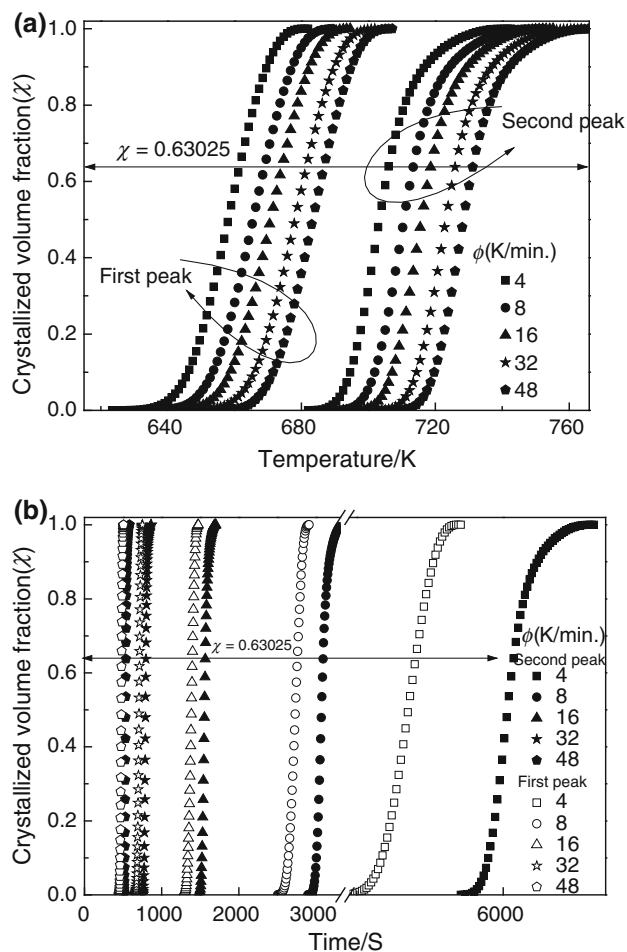


Fig. 9 The crystallized volume fraction as a function of **a** temperature and **b** time for the first and second peak of the glass 70 TeO₂-10 PbO-20 MnO₂ glass

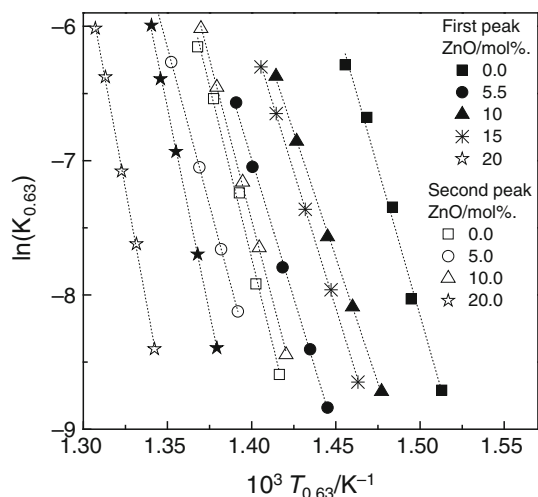


Fig. 10 The thermal parameter $\ln(K_{0.63})$ as a function of $10^3/T_{0.63}$ for 70 TeO₂- x ZnO-(20 - x) MnO₂-10 PbO ($0 \leq x \leq 20$ mol%) glasses

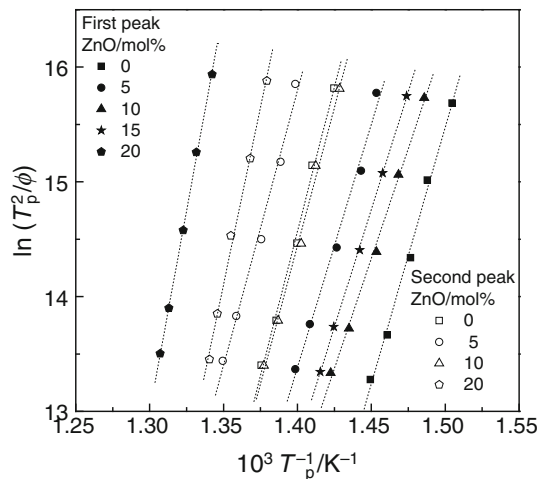


Fig. 11 The thermal parameter $\ln(T_p^2/\phi)$ versus $10^3/T_p$ for 70 TeO₂- x ZnO-(20 - x) MnO₂-10 PbO ($0 \leq x \leq 20$ mol%) glasses

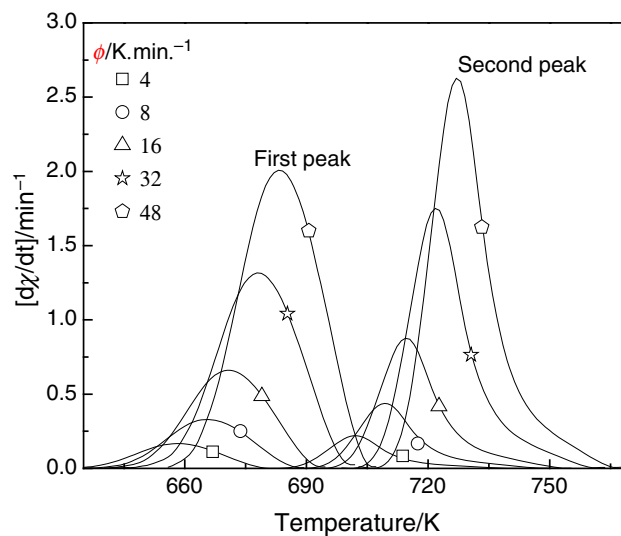


Fig. 12 Crystallization rate $(dx/dt)_p$ as a function of heating rate (ϕ) of the glass 70 TeO₂-10 PbO-20 MnO₂ glass

Figure 11 shows the plots of $\ln(T_p^2/\phi)$ versus $10^3/T_p$ for different glasses under study. The obtained values of the E_c and K_o as well as those obtained from Fig. 9.

The area under the DTA curve is directly proportional to the total amount of the crystallized alloy. The ratio between the ordinates and the total area of the peak gives the corresponding crystallization rates, which make it possible to plot the curves of the exothermal peaks represented in Fig. 12. It may be observed that the $(d\chi/dt)_p$ values increase with the increase of the heating rates, a property which has been widely discussed in the literature [32, 36]. With the aim of the correct application of the preceding theory, the materials were reheated up to a temperature

slightly higher than T_g for 1 h in order to form a large number of nuclei. It was confirmed by X-ray diffraction that the absence of any sharp line or crystalline peaks after the nucleation treatment for different compositions of the glass system $70 \text{ TeO}_2-x \text{ ZnO}-(20-x) \text{ MnO}_2-10 \text{ PbO}$ ($0 \leq x \leq 20 \text{ mol\%}$) i.e., a large number of nuclei exist already in the material, and therefore $m = n$ for the glasses under study. From the experimental data, it has been observed that the correlation coefficients of the corresponding straight regression lines showed a maximum value for a given temperature, which was considered as the most adequate one for the calculation of parameter n using the following relationship [37]:

$$\left(\frac{d\chi}{dt}\right)_p = n(0.37 \varphi E_c) / (RT_p^2). \quad (7)$$

The numerical factors n and m depended on the mechanism of nucleation, growth, and the dimensionality of the crystal. From the mean value of the kinetic exponent $\langle n \rangle$, it is possible to postulate a crystallization reaction mechanism. It was observed that n may be 4, 3, 2, or 1, which are related to different crystallization mechanisms: $n = 4$, volume nucleation, three-dimensional growth; $n = 3$, volume nucleation, two-dimensional growth; $n = 2$, volume nucleation, one-dimensional growth; and $n = 1$, surface nucleation, one-dimensional growth from surface to the inside [34–39]. From Table 2 one can notice that activation energy of crystallization of the first peak E_{c1} decreased with increasing ZnO content up to 10 mol%, and then it was increased with further increase of ZnO content. Also the values of E_{c2} take the same behavior but it disappeared at 15 mol% ZnO content.

Discussions

FTIR analysis

Kaur et al. [28] and El Mallawany [40] reported that the structure of TeO_2 -rich glasses consisted of trigonal bipyramidal (tbp) TeO_4 , deformed TeO_4 , TeO_{3+1} polyhedron, and trigonal TeO_3 pyramid (tp) structural units. The two highly mobile axial bonds (Te-O_{ax}) in each TeO_4 structural unit can be easily changed by network modifier atoms, and TeO_4 will be converted into TeO_3 . The formation of TeO_3 may be attributed to the elongation of the bond length of one of Te-O_{ax} bonds beyond 0.298 nm. Moreover, it was well established that the addition of lighter cations in a glass network shifted the vibrations of the bands to higher wave numbers. Thus, the values of the deconvoluted peaks of the studied glass system agree well with that reported elsewhere [31, 40, 41]. As shown in Figs. 1–3, the spectra of the studied glasses did not indicated the presence of the

characteristic bands at $\sim 400\text{--}460 \text{ cm}^{-1}$ of ZnO_4 or MnO_4 structural units [41]; thus, the former role of these units in the studied glasses can be, therefore, excluded.

In binary lead tellurite glasses [31], there is a transition between TeO_4 tbp and TeO_3 tp structures when modifier content increases. It is well known that the structural characteristic of tellurium atoms is related to the glass-forming ability (GFA) of this system: when modifier content increases, resulting TeO_3 structures and its non-bridging oxygen atoms turns difficult the glass formation. Due to its former role, addition of MnO_2 into the lead tellurite glasses contributed in the transformation of TeO_3 into TeO_4 structural units. Therefore, the area of equatorial and axial $[\text{TeO}_4]$ structural units indicated that these units were the main units in the manganese lead tellurite network. Moreover, the bond strength of Mn-O is higher than that of Zn-O [42]. As the ZnO content increases, the area of the band at $\sim 472 \text{ cm}^{-1}$ decreases and its frequency of vibration remains unvaried in the range of $0 \leq x \leq 10 \text{ mol\%}$. Beyond this limit, the area increases and the vibration of the band was shifted to lower frequencies indicating a substitution of MnO_6 by ZnO_6 structural units. The other characteristic tellurite bands were affected by the increase of ZnO content as follows.

The bands of TeO_4 were shifted to higher wavenumbers and their area increased in the range of $0 \leq x \leq 10 \text{ mol\%}$, and the bands of TeO_3 were shifted to lower wavenumbers along with a decrease in their area. This process indicates that there is a transformation of TeO_3 into TeO_4 and a more creation of bridging oxygens [38, 39].

As the ZnO content is increased beyond this limit, there is a suppression of TeO_4 as a consequence of the structural distortion due to the transformation of TeO_4 trigonal bipyramid into TeO_3 trigonal pyramid and TeO_{3+1} polyhedron structure [40, 41] which contributes to the increase in NBO as indicated by the shift of the bands of TeO_3 toward higher wavenumbers along with an increase in their area on the contrary of the assigned bands of TeO_4 .

On the other hand, detection of ZnO_6 structural unit in the studied glass network indicated the existence of connected NBO to ZnO_6 octahedral unit and ZnO acts as a modifier. Thus, these oxygens break the local symmetry of the Te-O-Te bonds. It is suggested that in this condition, Zn^{2+} ions may occupy interstitial positions and form weak ionic Zn-O bond [42] which may also contribute to the decrease of the rigidity of the glass [43].

Differential thermal analyzer (DTA) studies

The results shown in Fig. 7 indicate the validity of Eq. (1) for the all glasses under study, and the increase of T_g with the heating rate along with its decrease with increasing ZnO content is confirmed. Therefore, the observed

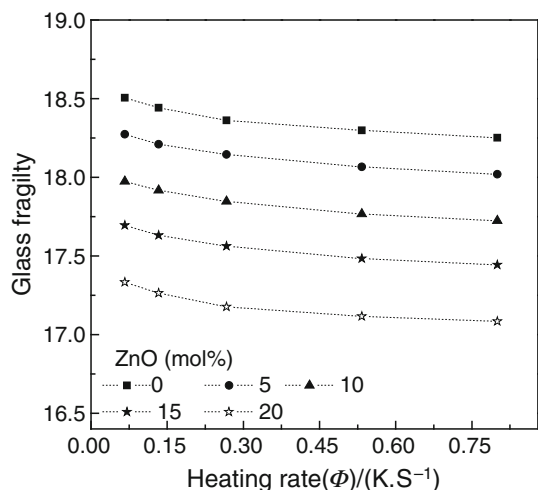


Fig. 13 Glass fragility (F) as a function of heating rate (ϕ) 70 TeO₂- x ZnO-(20 - x) MnO₂-10 PbO ($0 \leq x \leq 20$ mol%) glasses

decrease in the activation energy of glass transition as an apparent decrease in the T_g values can be ascribed to the increase in ZnO₆ structural units which is accompanied with the creation of NBO, i.e., ZnO acts as a glass modifier. Another reason for this decrease can be attributed to the influence of formed weak Zn-O bonds as indicated from the shift of structural units TeO₃ and TeO₃₊₁ to higher wavenumber confirming the weakening of lead tellurite network. The shift of the tellurite structural units was likely observed elsewhere [41]. The observed decrease in the values of E_g is found in good agreement with those previously reported by Pascuta et al. [23]. They found that when ZnO molecules were replaced by MnO in MnO-P₂O₅-ZnO glass, the E_g values decreases.

The above results can also be discussed on the basis of a parameter called fragility (F), which characterizes and quantifies the anomalous non-Arrhenius transport behavior of glassy materials near the ergodicity breaking glass transition region [23, 44]. Fragile glasses are substances with non-directional interatomic/intermolecular bonds. Strong glasses are those which show resistance to structural degradation and is usually associated with a small ΔC_p . Fragility (F) is calculated using the following relation [23]:

$$F = \frac{E_g}{T_g R \ln(1.01)} \quad (8)$$

The values of (F) decreased with the increase in ZnO content. This behavior indicates that the glasses become more fragile, and their tendency to structural rearrangement increases with increasing non-directional interatomic bonds. The values of the fragility index obtained for the studied glasses at different heating rates and ZnO content are shown in Fig. 13. Studying of structural relaxation in the glass transition region of glass-forming liquids has

great attention from both academic and technological points of view. Structural relaxation processes in glasses occur at temperatures lower than their T_g . Glass-forming liquids are defined as fragile glass former exhibiting non-Arrhenius temperature dependence of the viscosity, while that exhibiting Arrhenius behavior is known as strong glass formers. Fragile glasses have higher ionic bond character as compared to covalent bond component. The limit for kinetically fragile glass-forming (KF) liquids is characterized by a high value of F ($F \approx 200$) [23, 44], while the limit for kinetically strong glass-forming (KS) liquids is reached for a low value of F ($F \approx 16$) [44, 45]. Strong glasses are that showed a resistance to a structural degradation in the liquid state. For the 70 TeO₂- x ZnO-(20 - x) MnO₂-10 PbO ($0 \leq x \leq 20$ mol%) glasses, the values of F are near to KS limit. This indicates that all the glasses in the present study are obtained from KS liquids. Hence, stable glass with higher GFA required less activation energy for glass transition process [46]. In energy point of view, the state of an amorphous system, which has the lowest energy, is the best stable and is the best GFA. Larger activation energy for the glass transition (E_g) corresponds to larger fragility parameter (F). This reflects that the thermal stability of glasses and the stability of super-cooled liquids are attributed to the strong-fragile characteristics of glass-forming liquids.

The process of glass transition on heating the glass samples, turns the glassy state into super-cooled liquid state, is a process of atomic diffusion. A high thermal stable glass has a difficult atomic diffusion, i.e., the probability of the occurrence of nuclei growth is low; thus, the glass transition needs more time and the glass is high GFA. The total relaxation time for the glass transition can be estimated as ($\tau_{T_g} = \Delta T_g / \phi$), where ΔT_g is the difference between the onset and end points of T_g as determined from DTA curves [47]. The obtained values of τ_{T_g} as a function of ZnO at heating rate 8 K min⁻¹ are listed in Table 2. It was observed that the value of τ_{T_g} increases with increasing ZnO content. Accordingly, the GFA of the 70 TeO₂- x ZnO-(20 - x) MnO₂-10 PbO ($0 \leq x \leq 20$ mol%) glasses ranks from low to high ability as the ZnO content increases.

The observed decrease in values of E_{c1} and E_{c2} as listed in Table 2 indicates increasing the kinetic resistance toward the crystallization with the addition of ZnO up to 10 mol%. The glass sample containing 15 mol % ZnO having only one crystallization peak with activation energy (81.61 kJ mol⁻¹). This value of E_c is higher than that observed for the E_{c1} values of glassy samples with ZnO ≤ 10 mol%. Further addition of ZnO leads to increasing the kinetic resistance toward the crystallization that is obviously clear by sharp increase in T_p values and consequentially the E_c . The variation of the rate of growth, K_0 , is found in

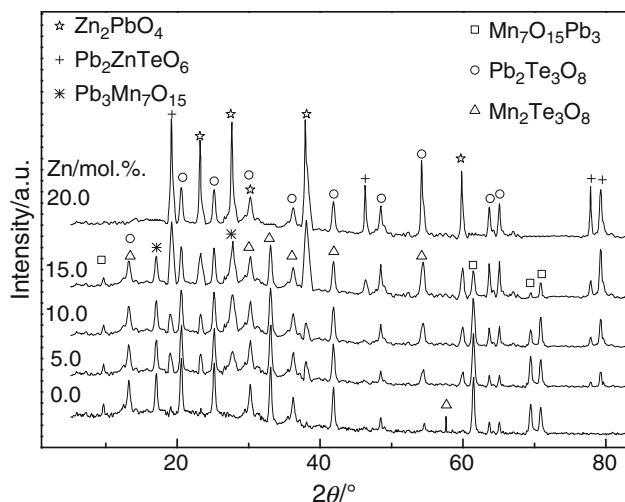


Fig. 14 XRD of annealed 70 TeO₂-*x* ZnO-(20 - *x*) MnO₂-10 PbO (0 ≤ *x* ≤ 20 mol%) glasses at the onset temperature of the first peak of crystallization for 2 h

accordance with the variation of T_p or E_c with increasing ZnO content (Table 2) that might give more understanding for the investigated glasses. Since K_0 is a measure of the growth rate of the crystallization process, it can be seen that the growth rate increases for all the investigated glass samples by increasing the heating rate and that in accordance with the above results of the crystallization rate (Fig. 12). While Table 2 measures the variation of K_0 with ZnO content that shows a decrease of K_0 by increase ZnO content up to 10 mol%. As far as it is known, the application of a controlled crystallization process required an attention to be paid to both nucleation and growth rates. Therefore, the reason for the preceding behavior of the investigated glass samples may be attributed to the retarded initial nucleation process with the increase of ZnO content up to 10 mol%. As discussed before, up to 10 mol % of ZnO and TeO₃ were transformed into TeO₄ structural units, i.e., the chance for nucleation process was low. Further increasing ZnO content more than 10 mol%, the Zn²⁺ ions were settled interstitially which helps increasing the crystal growth rate and increase the nucleation process.

The XRD diffractograms of the crystallized glass samples suggested the presence of microcrystallites involving three phases. According to the ICDD View 2006 identification cards,¹ these peaks can be identified as follows: (1) Pb₂Te₃O₈, (2) Mn₂Te₃O₈, (3) Mn₇O₁₅Pb₃, (4) Pb₂ZnTeO₆,

¹ ICDDVIEW 2006 identified cards these phases can be identified as (1) Pb₂Te₃O₈ (card No. 01-083-2228, 00-044-0568), (2) Pb₃Mn₇O₁₅ (card No. 00-036-0840, 01-076-0437, 01-077-1871, 01-070-1338), (3) Mn₂Te₃O₈ (card No. 01-072-0472, 00-024-0472 and 00-019-1172), (4) Pb₂ZnTeO₆ (card No. 00-029-1429 and 00-052-1792), and (5) Zn₂PbO₄ (card No. 00-023-1497 and 00-023-1496 and 00-023-1497).

and (5) Zn₂PbO₄, whereas an additional amorphous phase also remains, as shown in Fig. 14.

Conclusions

Different compositions of the 70 TeO₂-*x* ZnO-(20 - *x*) MnO₂-10 PbO (0 ≤ *x* ≤ 20 mol%) glasses have been synthesized. The results of FTIR and DTA were analyzed to study the effect of ZnO content on the structure and thermal analysis of these glasses. It was found that the lead tellurite network is the main network for the studied glasses. Furthermore, ZnO₆ structural unit has been detected in the studied glass network indicating the existence of connected NBO to ZnO₆ octahedral unit, and ZnO acts as a modifier. Thus, these oxygens break the local symmetry of the Te-O-Te bonds. The glass transition activation energy and glass fragility are found to decrease with increasing ZnO oxide ascribed to the formation of weak ionic Zn-O bonds at the expense of Mn-O bonds. Increasing ZnO up to 10 mol% is found to be decreasing the kinetic resistance toward the crystallization process, while increasing ZnO beyond this limit leads to an increase of the kinetic resistance toward the crystallization. This behavior was confirmed by the appearance of some crystallites like as Pb₂Te₃O₈ in all annealed glass samples. There are some crystallites that are formed with the addition of ZnO like as Pb₂ZnTeO₆ and Zn₂PbO₄ at the expense of Mn₇O₁₅Pb₃ or Mn₂Te₃O₈.

Acknowledgements Authors are highly thankful to Al-Azhar University for financial support.

References

- Lambson EF, Saunders GA, Bridge B, El-Mallawany RA. The elastic behaviour of TeO₂ glass under uniaxial and hydrostatic pressure. *J Non-Cryst Solids*. 1984;69(1):16.
- Saddeek YB. Structural and acoustical studies of lead sodium borate glasses original research article. *J Alloys Compd*. 2009;467(1-2):7.
- Sidkey MA, El Mallawany RA, Abousehly AA, Saddeek YB. Relaxation of longitudinal ultrasonic waves in some tellurite glasses. *Mater Chem Phys*. 2002;74(2):7.
- Aly KA, Dahshan A, Saddeek YB. Effect of MoO₃ additions on the thermal stability and crystallization kinetics of PbO-Sb₂O₃-As₂O₃ glasses. *J Therm Anal Calorim*. 2010;100(2):543-9.
- Niyaz Ahamad M, Vaish Rahul, Varma KBR. Calorimetric studies on 2TeO₂-V₂O₅ glasses. *J Therm Anal Calorim*. 2011;105:239-43. doi:10.1007/s10973-011-1305-3.
- Souri D, Salehizadeh SA. Glass transition, fragility, and structural features of amorphous nickel-tellurate-vanadate samples. *J Therm Anal Calorim*. 2013;112:689-95. doi:10.1007/s10973-012-2613-y.
- Yin D, Qi Y, Peng S, Zheng S, Chen F, Yang G, et al. Er³⁺/Tm³⁺ codoped tellurite glass for blue upconversion—structure, thermal stability and spectroscopic properties. *J Lumin*. 2014;146:8.

8. Shaaban ER, Saddeek YB, Abdel Rafea M. Crystallization kinetics of the TeO_2 -BaO glass system. *Phil Mag.* 2009;89(1):12.
9. Kasztelaniec R, Kujawa I, Stępień R, Haraśny K, Pysz D, Buczyński R. Molding of soft glass refraction mini lens with hot embossing process for broadband infrared transmission systems. *Inf Phys Technol.* 2013;61:6.
10. Hirashima H, Arari D, Yoshida T. Electrical conductivity of $\text{PbO-P}_2\text{O}_5\text{-V}_2\text{O}_5$ glasses. *J Am Ceram Soc.* 1985;68(9):3.
11. Khanna A, Bhatti SS, Singh KJ, Thind KS. Gamma-ray attenuation coefficients in some heavy metal oxide borate glasses at 662 keV. *Nucl Instrum Methods B.* 1996;114(3-4):3.
12. Rajendran V, Palanivelu N, El-Batal HA, Khalifa FA, Shafi NA. Document Effect of Al_2O_3 addition on the acoustical properties of lithium borate glasses. *Acoust Lett.* 1999;23(6):8.
13. Gautam CR, Kumar D, Parkash O, Singh P, Synthesis IR. Crystallization and dielectric study of (Pb, Sr)TiO₃ borosilicate glass-ceramics. *Bull Mater Sci.* 2013;36(3):8.
14. Ardelean I, Simon S, Peteanu M, Simon V, Ciorcas F, Bob C. Magnetic susceptibility studies on $\text{Bi}_2\text{O}_3\text{-PbO-As}_2\text{O}_3\text{-MnO}$ glasses. *Mater Lett.* 1999;39(1):3.
15. Saddeek YB, Yahia IS, Dobrowolski W, Kilanski L, Romčević N, Arciszewska M. Infrared, Raman spectroscopy and ac magnetic susceptibility of $\text{Gd}_2\text{O}_3\text{-TeO}_2\text{-V}_2\text{O}_5$ glasses. *Optoelectron Adv Mater Rapid Commun.* 2009;3(6):5.
16. Yahia IS, Saddeek YB, Sakr GB, Knoff W, Story T, Romčević N, et al. Spectroscopic analysis and magnetic susceptibility of $\text{CuO-TeO}_2\text{-V}_2\text{O}_5$ glasses. *J Magn Magn Mater.* 2009;321(24):5.
17. Sandhya Rani P, Singh R. Electron spin resonance and magnetization studies of $\text{ZnO-TeO}_2\text{-Fe}_2\text{O}_3$ glasses. *J Phys Chem Solids.* 2013;74(2):5.
18. Ardelean I, Hong-Hua Qiu, Sakata H. Magnetic properties of $\text{Fe}_2\text{O}_3\text{-Sb}_2\text{O}_3\text{-TeO}_2$ glasses. *Materials Letters.* 1997;32(5-6):3.
19. Giehl JM, Pontuschka WM, Barbosa LC, Ludwig ZMC. EPR of γ -induced paramagnetic centers in tellurite glasses. *J Non-Cryst Solids.* 2010;356(35-36):5.
20. Thomas RL, Nampoori VPN, Radhakrishnan P, Thomas S. Laser induced fluorescence in europium doped zinc tellurite glasses. *Int J Light Electron Optics.* 2013;124(22):2.
21. Srinivasa Reddy M, Murali Krishna G, Veeraiah N. Dielectric relaxation and a.c. conduction phenomena of $\text{PbO-PbF}_2\text{-B}_2\text{O}_3$ glasses doped with FeO. *J Phys Chem Solids.* 2006;67(11):11.
22. Upender G, Chandra Mouli V. Optical, thermal and electrical properties of ternary $\text{TeO}_2\text{-WO}_3\text{-PbO}$ glasses. *J Mol Struct.* 2011;1006(1-3):6.
23. Pascuta P, Bosca M, Borodi G, Culea E. Thermal, structural and magnetic properties of some zinc phosphate glasses doped with manganese ions. *J Alloys Comp.* 2011;509(11):5.
24. Saddeek YB, Shaaban ER, Abdel-Rahim FM, Mahmoud KH. Thermal analysis and infrared study of $\text{Nb}_2\text{O}_5\text{-TeO}_2$ glasses. *Phil Mag.* 2008;88(25):14.
25. Saddeek YB. Network structure of molybdenum lead phosphate glasses: Infrared spectra and constants of elasticity. *Physica B.* 2011;406(3):4.
26. Stuart B. Infrared spectroscopy: fundamentals and applications. Chichester: Wiley; 2004.
27. Ivanova Y. Phase equilibria in the MnO-TeO_2 system. *Mater Chem.* 1982;7(4):4.
28. Kaur A, Khanna A, Pesquera C, Gonzalez F, Sathe V. Preparation and characterization of lead and zinc tellurite glasses. *J Non-Cryst Solids.* 2010;356(18-19):8.
29. Bratu I, Ardelean I, Barbu A, Mih V, Maniu D, Botezan G. Spectroscopic and photoacoustic investigation of $x(\text{V}_2\text{O}_5\text{-CuO})(1-x)[3\text{B}_2\text{O}_3\text{-K}_2\text{O}]$ glasses. *J Mol Struct.* 1999;482-483:675-678.
30. Munoz-Martín D, Villegas MA, Gonzalo J, Fernández-Navarro JM. Characterisation of glasses in the $\text{TeO}_2\text{-WO}_3\text{-PbO}$ system. *J Eur Ceram Soc.* 2009;29(14):10.
31. Silva M, Messaddeq Y, Ribeiro S, Poulain M, Villain F, Briois V. Structural studies on $\text{TeO}_2\text{-PbO}$ glasses. *J Phys Chem Solids.* 2001;62(6):5.
32. Ardelean I, Cora S, Lucacel R, Hulpus O. EPR and FT-IR spectroscopic studies of B_2O_3 single bond Bi_2O_3 single bond MnO glasses. *Solid State Sci.* 2005;7(11):4.
33. Aziati S, Yahya AK, Halimah MK. Effects of Fe_2O_3 replacement of ZnO on elastic and structural properties of $80\text{TeO}_2\text{-(20-x)ZnO-xFe}_2\text{O}_3$ tellurite glass system. *J Non-Cryst Solids.* 2012;358(12-13):6.
34. Aly KA, Saddeek YB, Dahshan A. Effect of WO_3 on the glass transition and crystallization kinetics of borotellurite glasses. *Phil Mag.* 2010;90(33):12.
35. Kissinger HE. Variation of peak temperature with heating rate in differential thermal analysis. *J Res Nat Bur Stand.* 1956;57(4):4.
36. Afify N. A new method to study the crystallization or chemical reaction kinetics using thermal analysis technique. *J Phys Chem Solids.* 2008;69:6.
37. Shelby JE. Thermal expansion of amorphous metals. *J Non-Cryst Solids.* 1979;34(1):8.
38. Aly KA, Hassaan MY, Saddeek YB. Thermal features and physical properties of sulfur modified barium vanadate glasses. *Phase Transitions.* 2013;86(5):12.
39. Othman AA, Aly KA, Abousehly AM. Crystallization kinetics in new $\text{Sb}_{14}\text{As}_{29}\text{Se}_{52}\text{Te}_5$ amorphous glass. *Solid State Commun.* 2006;138(4):5.
40. El Mallawany RA. Tellurite glasses physical properties and data. New York: CRC Press; 2002.
41. Mohamed NB, Yahy AK, Deni MSM, Mohamed SN, Halimah MK, Sidek HAA. Effects of concurrent TeO_2 reduction and ZnO addition on elastic and structural properties of $(90-x)\text{TeO}_2\text{-10Nb}_2\text{O}_5\text{-(x)ZnO}$ glass. *J Non-Cryst Solids.* 2010;356(33-34):4.
42. Lide D. CRC handbook of chemistry and physics. 84th ed. FL: CRC Press, Boca Raton; 2004.
43. Baizura N, Yahya AK. Effects of Nb_2O_5 Replacement by Er_2O_3 on elastic and structural properties of $75\text{TeO}_2\text{-(10-x)Nb}_2\text{O}_5\text{-15ZnO-(x)Er}_2\text{O}_3$ glass. *J Non-Cryst Solids.* 2011;357(15):5.
44. Omar A, Lafi, Imran MA, Abdullah MK. Glass transition activation energy, glass-forming ability and thermal stability of $\text{Se}_{90}\text{In}_{10-x}\text{Sn}_x$ ($x = 2, 4, 6$ and 8) chalcogenide glasses. *Phys B.* 2007;395(1-2):6.
45. Viglis TA. Strong and fragile glasses: A powerful classification and its consequences. *Phys Rev B.* 1993;47(5):3.
46. Bohmer R, Angell CA, Richert R. Disorder effects on relaxation processes. In: Bluman editor. Berlin: Springer; 1994.
47. Mehta N, Tiwari RS, Kumar A. Glass forming ability and thermal stability of some Se-Sb glassy alloys. *Mater Res Bull.* 2006;41(9):8.